GEOPHYSICAL RESEARCH LETTERS, VOL. 26, NO.6, PAGES 647-650, MARCH 15, 1999

FAST observations of inertial Alfven waves in the dayside aurora

C. C. Chaston, C. W. Carlson, W. J. Peria, R. E. Ergun and J. P. McFadden
Space Sciences Laboratory, University of California, Berkeley

Abstract. Bursts of large amplitude impulsive electric and magnetic field oscillations are a common feature observed from FAST when crossing the dayside auroral oval at altitudes from 1500-2500 km. The oscillations have transverse amplitudes of up to 1 V/m and 100nT and exhibit a parallel electric field component with amplitudes which may be as large as 100mV/m. Calculation of $E_\parallel/B_\perp$ over 100 events yields an average value four times the local Alfven speed. The wave period is usually less than 0.25s with 'perpendicular wavelengths' which average to 7.1 electron skin depths (c/ω_{pe}~80m). Poynting flux calculations indicate predominately downward fluxes with magnitude up 10^{-2} Wm^{-2} usually accompanied by a smaller upwards component. Invariably these waves are accompanied by field-aligned fluxes of down going and sometimes counterstreaming suprathermal electrons. Comparison with theoretical studies indicate that these observations are consistent with the characteristics of a shear Alfven wave with $k_\perp \sim \omega_{pe}/c$ propagating in the inertial dispersive regime and interfering with a reflected component. However the observed large parallel electric field component, if real, has yet to be explained

Introduction

The occurrence of Alfven waves in the aurora has been reported from sounding rockets (Boehm et al., 1990, Knudsen et al., 1992) as well as spacecraft, including S3-3, Freja, and Viking (Mozer et al., 1977; Wahlund et al., 1994, Gustaffson et al., 1990, Aikio et al., 1996). These waves are identified with $E_\parallel/B_\perp$ ratios of the order of the Alfven speed and perpendicular scale sizes (defined as the distance travelled by the spacecraft perpendicular to the background magnetic field while observing one full oscillation) of afew electron skin depths (c/ω_{pe}). The observed waveforms are oscillations of one or more cycles or often a single impulsive deviation. In addition these waveforms may be significantly steepened as they propagate (Seyler et al., 1998) forming what has been identified from Freja spacecraft observations as SKAW (Solitary Kinetic Alfven Waves).

Wave and Plasma Observations

Figure 1 presents a summary of a FAST pass through the morning side edge of the cusp containing a burst of ultra low frequency turbulence composed of a series of spikes in E and B. The first panel shows that the electric field amplitude of the turbulence is several 100 mV/m and the second panel indicates B field amplitudes of 10s nT. These measurements provide $E_\parallel/B_\perp$ values close to $1x10^7$ ms^{-1} which is identical to the result reported by Louarn et al. (1994) for observations in the afternoon oval at similar altitudes. The third panel illustrates the spectra of low frequency turbulence observed from the rotating spacecraft. The impulsive structures essentially fill the band below the proton gyro frequency (Ω_p, indicated by the white line) and in some cases higher frequency fluctuations within the individual spikes extend above Ω_p.

The total electron density represented in the fourth panel is obtained from the Langmuir probe current which is calibrated using the observed frequency of the Langmuir emission coincident with the ultra low frequency turbulence. Higher resolution Langmuir probe data indicate density depletions in association with each waveform as reported previously by Boehm et al. (1990), Stasiewicz et al. (1998) and others, however the actual depth is uncertain. For calculation of the Alfven speed mass composition has been determined by assuming an O^+ -H^+ plasma and using the low frequency limit of the plasmaspheric hiss given by the L mode H^+ branch cutoff (Santolik and Parrot, 1998). In an O^+ rich plasma this frequency is located just below Ω_p as found in the third panel of Figure 1. Using this approach we find O^+ concentrations of between 80-90% yielding Alfven speeds ranging from $2\text{-}4x10^6 ms^{-1}$ over those times where the Alfvenic fluctuations appeared. The TEAMS mass spectrometer instrument at these times indicated total He^{++} densities of less than 1 cm^{-3}. The concentration of He^+ is unknown, however, the influence of this species on the Alfven speed can be expected to be small in an 80-90% oxygen plasma.

The fifth panel shows the field-aligned Poynting flux calculated from the 3D electric and magnetic field data. This shows that the energy associated with the waveforms propagates predominately downwards (+ve S_z) along the field with fluxes up to 10^{-2} Wm^{-2}, an order of magnitude larger than the transverse flux (not shown). Intervals of upward directed fluxes also occur (13:55:17 and 13:55:40) and may represent the reflection of an obliquely propagating Alfven wave at lower altitudes. Those Alfven disturbances whose Poynting flux is without a preferred direction have $E_\parallel/B_\perp$ values usually larger than those of the travelling waves. Superimposed on the Poynting flux is the calculated downgoing electron energy flux multiplied by 10 for scaling purposes. The more intense Poynting fluxes appear to be well correlated with instances of enhanced energy flux.

The corresponding particle data is contained in the bottom four panels. The electron energy spectra indicates that the enhanced wave turbulence is coincident with the appearance of suprathermal fluxes with energies up to 1 keV. The pitch angle data show that these electrons are strongly field-aligned (0°) and in some cases counterstreaming (180°). The ion data presented in the two lowest panels of Figure 1 is influenced at energies below 100eV by ram effects indicated by the disproportionately high fluxes below this energy at ~90° or 270°. Nonetheless the presence of magnetosheath ions identified by the energy/latitude dispersion in the energy range from 10 keV-100eV (Heikkila and Winningham, 1971; Phillips et al., 1993) seen after 13:55:25 UT and the presence of He^{++} ions locates the spacecraft in the morningside edge of the cusp or the flank boundary layer. The dropout of electrons at energies above 1 keV starting at 13:54:55 UT is also consistent with this interpretation. The last panel shows evidence for transverse energization of ions indicated by

Paper number 1998GL900246.
0094-8276/99/1998GL900246$05.00

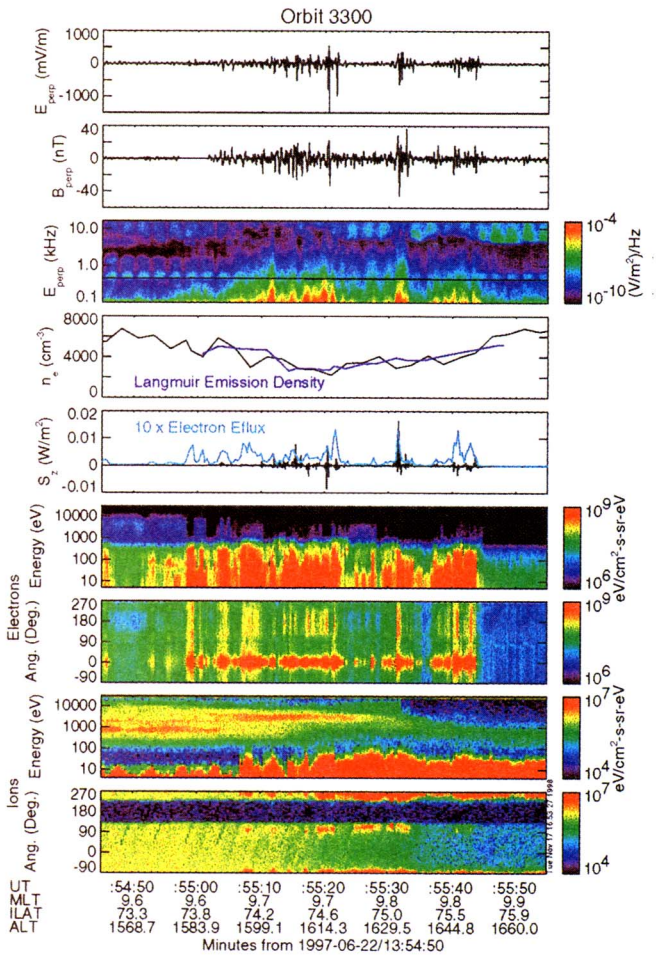

Figure 1. Alfven waves and particle observations. The first panel shows the detrended electric field perpendicular to B_0 and to the spacecraft trajectory. The second panel shows the magnetic field measured by the fluxgate magnetometer above 1 Hz perpendicular to B_0 and to the electric field in the first panel. A data gap occurs in this panel at 13:54:55 UT. The third panel contains the dynamic power spectrum of the electric field in the spin plane up to 16 kHz. The fourth panel contains the density from the Langmuir probe calibrated using the density inferred from Langmuir waves often observed coincident with bursts of Alfvenic activity. The fifth panel contains the field-aligned Poynting flux where positive values indicate downward energy flux. Overplotted on this panel is the integrated downward electron energy flux mutiplied by 10. The sixth panel shows the electron energy spectra, the seventh shows the electron pitch angle spectra, the eigth shows the ion energy spectra and the ninth shows the ion pitch angle spectra.

enhanced fluxes at ~90° as discussed by Knudsen and Wahlund (1998) using observations from the Freja spacecraft.

Figure 2 provides a closer look at the observed waveform of a single impulsive event. The coordinate system is field-aligned with the x-component perpendicular to the spacecraft trajectory and pointing roughly westwards, the y-component points along the spacecraft trajectory or northwards and the z-component is along the field and pointing downwards. The electric field data indicate that the disturbance contains a rich spectrum of field variations with the lowest frequency component having a period of the order of 0.2s in the spacecraft frame and an amplitude of 500 mV/m. The same waveform is apparent in the fluxgate magnetometer measurement. The lowpass filtered time series (<20Hz) (indicated by the red lines in the first two panels of Figure 2a) allow an approximate phase relation to be determined. Close inspection reveals that E_x and B_x are ~$\pi/2$ out of phase, E_x and B_y are close to in phase, E_y and B_x are close to in phase and E_y and B_y are ~$\pi/2$ out of phase. These phase differences and the fact that there is no B_z wavefield are consistent with a travelling shear Alfven wave interpretation.

Plotting the B_x/B_y hodogram indicates right-handed elliptical polarization consistent with that from a cylindrical current system as investigated by Volwerk et al. (1996). The blue lines on magnetic field times series in Figure 2a indicate the modeled magnetic field seen by a spacecraft traversing such a system. This consists of a core upwards current in the centre with a radius of 350m through which

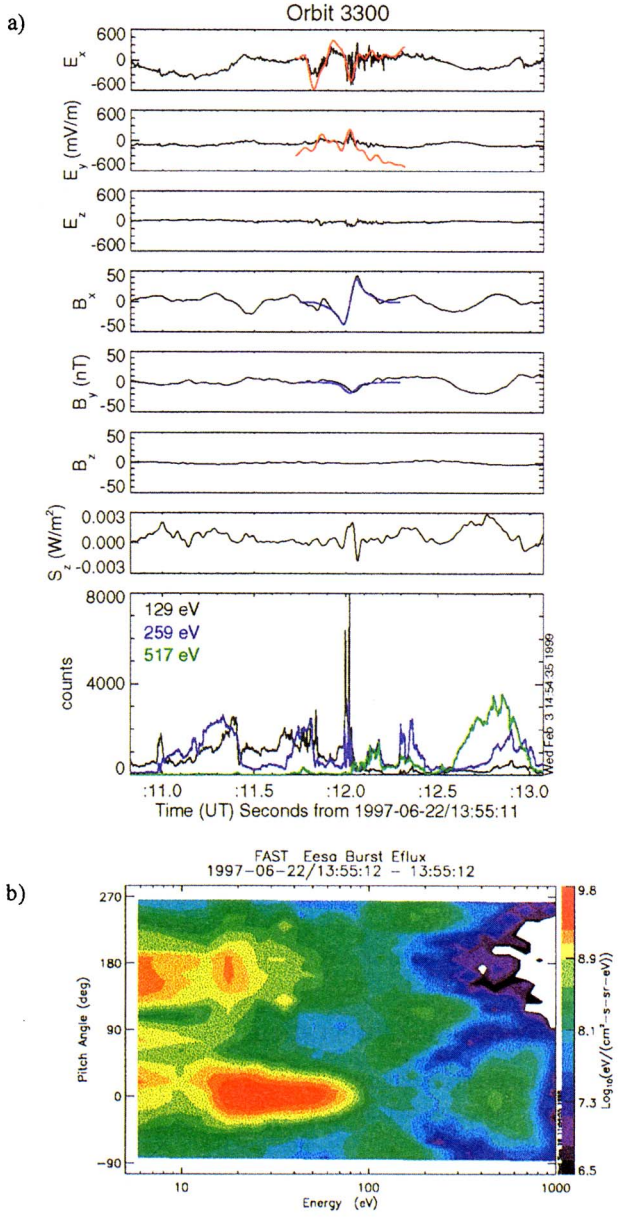

Figure 2. Microphysics of an auroral Alfven wave. In 2(a) the first six panels show the 3D electric and magnetic field components in a field-aligned coordinate system with positive Z downwards. The red lines are the low pass filtered electric field (20 Hz cutoff) amplified to fill the scale. The blue lines are the simulated magnetic field time series discussed in the text. The seventh panel shows the field-aligned Poynting flux with positive values pointing downwards. The eigth shows the counts recorded in field-aligned (-22.5° to 22.5°) fixed energy channels. 2(b) presents the distribution function in units of differential energy flux observed coincident with the solitary Alfven wave at 13:55:12 UT.

the spacecraft passes at 13:55:12UT and a coaxial return sheath with a radius of ~1.5 km. To obtain magnetometer deflections of amplitudes similar to those observed requires a total current of ~60A yielding a current density through the core of 150 $\mu A/m^2$. Inspection of the higher resolution induction magnetometer data for this and other events reveals that the higher frequency electric field oscillations observed within the Alfven wave are also present in the magnetic field however with amplitudes that fall rapidly with increasing wave frequency above 50 Hz.

There is a significant field-aligned component in the electric field with a uni-polar magnitude of 50-100 mV/m directed upwards although bi-polar parallel electric field components are also observed in other cases with equal regularity. Similar parallel fields within Alfvenic disturbances have been reported by Stasiewicz et al. (1998). For the event illustrated one of the three orthogonal E-field dipoles was within 2.4° of the model background field making the contribution from the perpendicular fields along this direction small. Determing the parallel field with alternative sphere pairs yields amplitudes along $\mathbf{B_0}$ within 50% of that given in Figure 2. Nonetheless, due to the large number of instrumental effects that can give false signatures, this result still cannot be considered certain.

The field-aligned Poynting flux illustrated in the seventh panel of figure 2a shows a positive peak (downwards) coincident with a peak in the counts recorded in field-aligned electrons (-22.5° to 22.5°, downgoing) represented in the eigth panel at ~13:55:12 UT. The enhancement is measured in energy channels centered on 129 and 259 eV. The region of enhanced counts is limited to where a finite E_z is recorded and that region where the gradient in the transverse magnetic field is greatest. This low energy field-aligned burst constitutes an enhancement the upward current consistent with the direction inferred from the fluxgate magnetometer deflection with most of the current carried by electrons below the minimum energy of the analyser. The width of the region in which the acceleration occurs is of the order of 500m or approximately six times the electron skin depth.

Figure 2b illustrates an 80ms snapshot of the electron distribution captured during the enhancement. The measured distribution is dominated by a down going field-aligned (0°) electron beam with energies from 10 to 100 eV. A counterstreaming upward field-aligned beam (180°) of lower energy is also evident presumably representing the mirrored/backscattered component of the primary downgoing beam. At energies above 200 eV the usual inverted-V electrons and electron loss cone occur. The inverted-V feature observed throughout is represented in Figure 2a by the broader features in the 259 and 517 eV channels.

Phase Speeds and Scale Sizes

Figure 3 presents (a) $E_\perp/B_\perp$ values and (b) perpendicular scale sizes from a sample of 100 wave events over a range of altitudes from 1500 km to 2300 km and from 0900-1500 MLT. All observations included occurred coincident with magnetosheath ion precipitation. The $E_\perp/B_\perp$ results have been calculated using the transverse peak-peak amplitudes of the lowest frequency field variations within each event. These values may be in error by up to 25% due to contribution from higher frequency electrostatic fluctuations observed within the lower frequency structures. Scale sizes ($W_\perp$) are based on the assumption of a stationary structure and represent the perpendicular distance traversed by FAST for a complete cycle of the lowest frequency component of the waveform in the electric field. Many of the events contain more that one cycle. Narrower structures often exist within the broader features as has been reported from Freja (Wahlund et al. 1994). The $E_\perp/B_\perp$ results are plotted against the Alfven speed and the scale size results normalized by the electron skin depth. The value of Alfven speed and skin depth have been calculated individually for each event using the density and composition data determined from the techniques discussed in the previous section.

The range of $E_\perp/B_\perp$ values observed extend from 0.7-14 V_A with an average value of 3.99 V_A (1.0e7ms^{-1}). Each point in Figure 3a has been plotted with a symbol indicating the direction of its Poynting flux. The trend lines indicate that in general those waves having no preferred direction (standing) or an upwards directed Poynting flux have larger $E_\perp/B_\perp$ values. The condition $E_\perp/B_\perp=V_A$ provides a lower limit on the plotted results with only two events in the sample having a value less than V_A. The horizontal lines indicate the required ionospheric height-integrated Pedersen conductivity (Σ_p) for interpretation of these features as static narrow field-aligned currents (Sugiura et al., 1984). These values are much less than observed for a sunlit ionosphere (Reiff, 1984) thereby making the field-aligned current interpretation improbable.

For the scale size results to be a useful indication of the perpendicular wavelength (i.e. $W_\perp \cong \lambda_\perp$) it is necessary that the wave phase should not alter by more than $\pi/2$ radians over the time it takes for FAST to traverse one wavelength. This in essence requires that the apparent phase speed along the spacecraft track (v_p) is < 0.25 the spacecraft speed (v_s). Given that the FAST spacecraft traverses one cycle of the lowest frequency component in each structure in ~0.2 seconds this requires the wave frequency to be ≤ 1.25Hz It should also be noted that since the actual orientation between spacecraft

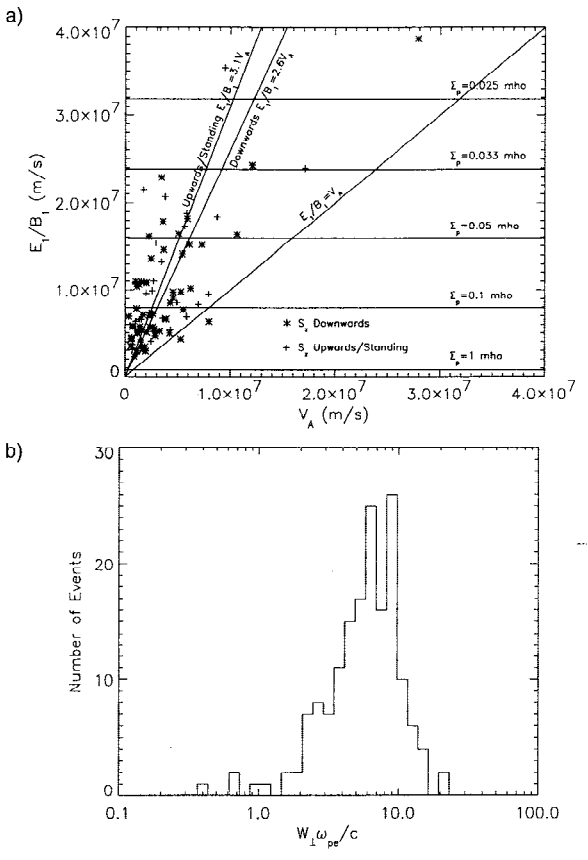

Figure 3. Wave properties. 3(a) shows the distribution of the ratio of the transverse electric to magnetic field plotted against the local Alfven speed. 3(b) shows the distribution of the perpendicular size of individual oscillations from the electric field normalised in terms of the electron skin depth (c/ω_{pe}).

track and $k_\perp$ is unknown this technique provides values for the measured perpendicular scale size with $W_\perp \geq \lambda_\perp$.

An estimate of the wave frequency can be determined by using interferometric techniques. Employing multiple dipole pairs indicates that these structures are close to stationary over the time taken for FAST to traverse the structure with v_p (~perpendicular to $\mathbf{B_0}$) of at most 1 kms^{-1}. The spacecraft velocity is at this time 7 kms^{-1}. The wave frequency is given by $\omega=[v_p/(v_p-v_s\cos\theta)]\omega_s$ where $\mathbf{v}_p$ and $\mathbf{v}_s$ are the wave phase velocity and spacecraft velocity both in the plane perpendicular to $\mathbf{B_0}$ and separated by angle θ. ω_s is the wave frequency in the spacecraft frame. From geometric considerations the maximum v_p is measured at those times when the spacecraft trajectory and $k_\perp$ are most closely aligned (i.e. θ=0). Under such conditions $v_p=v_p$ and so we can estimate a maximum frequency. The observed ω_s of the lowest frequency component is ~5 Hz. Substituting v_p=1 kms^{-1} into the expression above then provides an estimate of the maximum wave frequency of ~1 Hz. This frequency we believe is sufficiently low for the identifying the measured perpendicular scale size as an upper limit for $\lambda_\perp$ or for calculating a lower limit on $k_\perp=2\pi/\lambda_\perp$.

The distribution shown in Figure 3b covers a range $W_\perp\omega_{pe}/c$=0.63-17.6 with a mean of 7.1 (or $\bar{\lambda}_\perp$=590m) suggesting a minimum wavenumber of $\bar{k}_\perp c/\omega_{pe}$=0.88. This result can be compared to that derived from the inertial Alfven wave relation, $E_1/B_1=V_A(1+k_\perp^2c^2/\omega_{pe}^2)^{1/2}$ (Goertz and Boswell, 1979). Using this dispersion relation the trendline for downgoing waves in Figure 3a gives $k_\perp c/\omega_{pe}\approx$2.4, a value much larger than the minimum value determined from the scale size analysis. This suggests that either FAST trajectory is typically very oblique to $k_\perp$(thereby providing a larger measured $\lambda_\perp$), or significant modification of E_1/B_1 due to an interfering ionospherically reflected wave component, or that the pure plane wave approximation required for the above analysis is inaccurate for these waves. The modeling results of Lysak(1998) (Figures 2b and 2d of that paper) show that inclusion of a reflected interfering wave with $\lambda_\perp$=1 km and Σ_p=10 can explain the observed E_1/B_1 ratios.

Before closing some comment should be made regarding the large amplitude parallel electric field component observed in some cases. For an inertial Alfven wave the ratio $E_z/E_1=(k_\parallel k_\perp c^2/\omega_{pe}^2)/(1+k_\perp^2c^2/\omega_{pe}^2)$ predicts parallel field amplitudes (E_z) two orders of magnitude smaller than the observed values. In cases (such as Figure 2a) where higher frequency oscillations are observed within the Alfven wave, the parallel component may arise from anomalous resistivity as described by Lysak and Carlson (1981). In this case when the effective parallel collision frequency becomes much greater than the wave frequency the magnitude of the parallel potential approaches the perpendicular potential. However, for $k_\perp/k_\parallel$ of several hundred this gives at most parallel fields of afew mV/m. If real, then the large parallel component is most likely a feature associated with the non-linear evolution of the waveform.

Conclusion

Alfven waves propagating in the dayside auroral oval and in the vicinity of the cusp have been identified from FAST. These waves are observed to occur in narrow regions transverse to the field typically of the order of 3 km and have highly non-sinusoidal irregular wave forms. From the determination of the total electron density and ion composition using plasma wave observations over an altitude range from 1500-2300 km it is found that these waves have E_1/B_1 values which scale with the Alfven speed, with an average equal to four times the local value. In addition it is found that the field oscillations have perpendicular scale sizes of several electron skin depths with an average value of $\bar{W}_\perp$=590m $\geq\lambda_\perp$ or $\bar{k}_\perp c/\omega_{pe}\geq$0.88. These observations are similar to those reported from the Freja spacecraft at comparable altitudes.

Calculation of the Poynting flux associated with these disturbances using the 3 axis E and B fields measurements available on the FAST satellite indicates mainly downwards propagation with a weaker counterpropagating component thought to be associated with reflection at lower altitudes. Comparison with the results of Lysak (1998) indicates that the observed values of E_1/B_1 and $\lambda_\perp$ are consistent with this interpretation. However, the large parallel field electric field observed is not consistent with this interpretation and cannot be derived from finite electron inertia alone.

These waves are invariably accompanied by enhanced electron fluxes to several hundred eV distributed as narrow field-aligned beams. Observations of fixed energy channels indicate order of magnitude variations in counts observed with the passing of the waveform and no clear dispersive character, perhaps suggesting near local acceleration. These small scale Alfvenic structures may provide a means for electron acceleration over perpendicular widths sufficiently narrow to explain fine structure in auroral arcs in the dayside oval.

Acknowledgements. This research was motivated by discussions during the March 1998 ISSI Alfven wave workshop and supported by NASA under grant NAG-3596

References

Aikio, A. T., et al., On the origin of high altitude electric field fluctuations in the auroral zone, *J. Geophys. Res., 101,* 27157, 1996.

Boehm, M. H., et al., High-resolution sounding rocket observations of large-amplitude Alfven waves, *J. Geophys. Res., 95,* 12157, 1990.

Goertz, C. K., and R. W. Boswell, Magnetosphere-ionosphere coupling, *J. Geophys. Res., 84,* 7239, 1979.

Gustaffson, G., et al., On waves below the local proton gyro frequency in auroral acceleration regions, *J. Geophys. Res., 95,* 5889, 1990

Heikkila, W. J., and J. D. Winningham, Penetration of Magnetosheath plasma to low altitudes through the dayside magnetospheric cusps, *J. Geophys. Res., 76,* 883, 1971.

Mozer, F. S., et al., Observations of paired electrostatic shocks in the polar magnetosphere, *Planet. Space Rev., 38,* 292, 1977.

Knudsen, D. J., et al., Alfven waves and the auroral ionosphere: A numerical model compared with measurements, *J. Geophys. Res., 97,* 77, 1992.

Knudsen, D. J., and J. E. Wahlund, Core ion flux bursts within solitary kinetic Alfven waves, *J. Geophys. Res., 103,* 4157, 1998.

Louarn, P., et al., Observation of kinetic Alfven waves by the Freja spacecraft, *Geophys. Res. Lett., 21,* 1847, 1994.

Lysak, R. L. The relationship between electrostatic shocks and kinetic Alfven waves, *Geophys. Res. Lett., 25,* 2089, 1998

Phillips, J. L., et al., Well-Resolved observations by ISEE 2 of ion dispersion in the magnetospheric cusp, *J. Geophys. Res., 98,* 13429, 1993.

Reiff, P., Models of Auroral Conductances, in *Magnetospheric Currents,* ed. by T. A. Potemra, American Geophysical Union, Geophysical Monograph 28, 180, 1984.

Santolik, O., and M. Parrot, Propagation analysis of electromagnetic waves between the helium and proton gyro-frequencies in the low-altitude auroral zone, *J. Geophys. Res., 103,* 20469, 1998.

Seyler, C. E., et al., Electrostatic broadband ELF wave emission by Alfven wave breaking, *J. Geophys. Res., 103,* 7027, 1998.

Stasiewicz, K., et al., Density depletions and current singularities observed by Freja, *J. Geophys. Res., 103,* 4251, 1998.

Sugiura, M., et al., in *Magnetospheric Currents,* ed. by T. A. Potemra, American Geophysical Union, Geophysical Monograph 28, 96, 1984.

Volwerk, M., P. et al., Solitary kinetic Alfven waves: A study of the Poynting flux, *J. Geophys. Res., 101,* 13335, 1996.

Wahlund, J. E., et al.,On ion acoustic turbulence and the nonlinear evolution of kinetic Alfven waves in aurora, *Geophys. Res. Lett., 21,* 1831, 1994

C. W. Carlson. C. C. Chaston, R. E. Ergun, J. P. McFadden and W. J. Peria, Space Sciences Laboratory, University of California, Berkeley, CA 94720

(Received September 21, 1998; revised November 12, 1998; accepted November 16, 1998.)